Modeling of Thermal-Hydraulic Effects of AC Losses in the ITER Central Solenoid Insert Coil Using the M&M Code

Roberto Zanino, Laura Savoldi Richard, and Elena Zapretilina

***Abstract*—During 2000, AC losses and the effects of possible ramp-rate limitation (RRL) were investigated on the International Thermonuclear Experimental Reactor (ITER) Central Solenoid Insert Coil (CSIC), at JAERI Naka, Japan. The CSIC was mounted inside the bore of the ITER Central Solenoid Model Coil (CSMC), at the maximum field of about 13 T and experiencing the largest magnetic field variations. The thermal-hydraulic response of the coil to different transport current scenarios was assessed by measuring the temperature increase and pressurization of the supercritical helium (SHe) coolant, together with the evolution of the mass-flow rate. Here we implement in the M&M code a detailed general model of AC losses, which is being validated for the first time. The resulting tool is then applied to the analysis of two CSIC tests, with different ramp-up of the transport current followed by the same dump, and used to qualitatively assess the major thermal-hydraulic effects of AC losses in the coil.**

***Index Terms*—AC losses, computational thermal-hydraulics, fusion reactors, ITER, superconducting coils.**

I. Introduction

AC LOSSES are an essential item in the design and operation of superconducting magnets, because the associated heat source can lead to initiation of a normal zone and, possibly, to quench propagation in the superconductor. As a consequence, a significant part of the tests [1]–[3] performed during 2000 on the ITER CSIC, at JAERI Naka, Japan, was devoted to assessing the intensity and effects of AC losses.

The CSIC is a Nb3Sn single-layer solenoid, ~140 m long, wound one-in-hand and positioned inside the bore of the ITER CSMC, at the maximum field of ~13 T. The conductor is of the cable-in-conduit type with a thick square Incoloy jacket, and the dual-channel structure typical of ITER [1].

In order to assess the major thermal-hydraulic effects of AC losses in the CSIC, we implement here in the M&M code [4], a validated tool already used for thermal-hydraulic analysis of the ITER Model Coil experiments, a model for AC losses, already used for the predictive analysis of the ITER magnets [5], but validated here for the first time.

Manuscript received August 6, 2002. The work of R. Zanino and L. S. Richard was supported in part by the European Fusion Development Agreement and by Associazione per lo Sviluppo Scientifico e Tecnologico del Piemonte.

R. Zanino and L. Savoldi Richard are with the Dipartimento di Energetica, Politecnico, I-10129 Torino, Italy.

E. Zapretilina is with the ITER IT (as Visiting Personnel), Naka JWS, Japan, on leave from the Scientific-Research Institute of Electro-Physical Apparatus (NIIEFA, Efremov Institute), St. Petersburg, Russia (e-mail: zaprete@itergps.naka.jaeri.go.jp).

Digital Object Identifier 10.1109/TASC.2003.812687

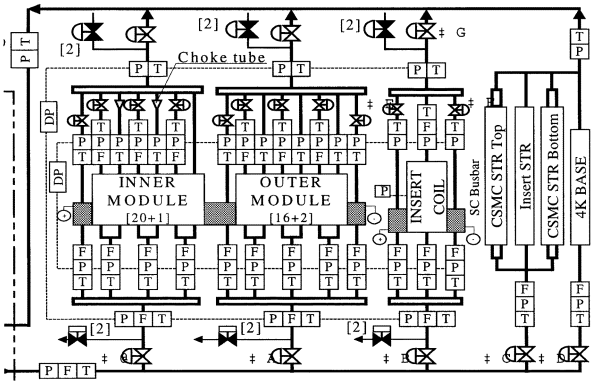

Fig. 1. Schematic view of the CSMC+CSIC hydraulic circuit. T, P, and F indicate temperature sensors, pressure taps, and flow meters, respectively.

II. Experimental Setup

The CSMC and CSIC tests are already described in detail elsewhere [1]–[3]. While AC losses were investigated using a standard trapezoidal cycle [3], the largest effects of these losses were clearly seen in the RRL tests, where the stability of the CSMC and CSIC conductors was tested under high rates of field variation (actually even beyond the original goal of 0.4 T/s) up to 13 T, using the power supplies of the JAERI tokamak JT-60 [1].

The CSIC is well diagnosed from the thermal-hydraulic point of view (see Fig. 1): the response of the coil to different scenarios of transport current variation can be assessed by measuring the temperature "T" and pressure "p" increase at the inlet, center and outlet of the conductor, together with the variation of the SHe coolant mass-flow rate at the inlet and outlet. The *whole* cryogenic circuit (parallel) of CSIC+CSMC, shown in Fig. 1, will play an essential role in the assessment of the thermal-hydraulic effects of AC losses in the CSIC.

III. Model

A. Thermal-Hydraulic Model

The thermal-hydraulic model used here is that implemented in the Multi-conductor Mithrandir (M&M) code [4]. M&M allows the simulation of thermal-hydraulic transients in coils with different complex topologies, e.g., layer wound as in the case of the CSMC [6], or pancake wound as in the case of the ITER Toroidal Field Model Coil [7]. The single-conductor model on which M&M is based, i.e., the Mithrandir model, was already successfully applied in the past to the analysis of stability and

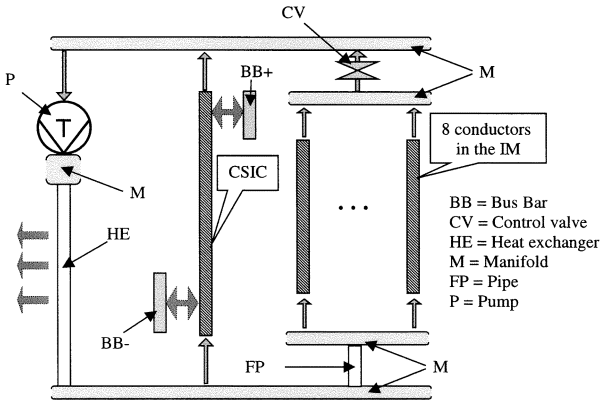

Fig. 2. Hydraulic circuit model adopted in the M&M simulations.

quench tests in the CSIC [8], [9]. However, in the case of longer time-scale transients as those considered here, the role of all the other channels, hydraulically in parallel with the CSIC, may be very important, so that the Mithrandir model may be insufficient, and M&M is needed.

Different models with increasing sophistication of the hydraulic circuit have been used here, from an open single conductor with experimental inlet (p and T) and outlet (T) boundary conditions, to a closed circuit including the hydraulic parallel of the CSIC, and of 8 conductors representing the four innermost layers of the inner module of the CSMC, as shown in Fig. 2. (In this case, also the thermal coupling between the CSIC and its superconducting busbars is taken into account.) In comparing the two approaches it may be said that the experimental boundary conditions are simplest in principle, but may in practice turn out to be too coarse (low sampling rate data) or too noisy (high sampling rate data). On the other hand, the full circuit model allows a more detailed analysis of the effects of the hydraulic parallel, as well as a validation of the *predictive* capabilities of the computational tool, although some of the quantities to be modeled, e.g., the mass flow rate evolution, can be very sensitive to parameters like the volume of the manifolds in the circuit, which is in turn affected by significant uncertainty.

B. AC Losses Model

The approach to the CS Insert AC-loss modeling is very similar to the one described in [10], but the model is being validated here for the first time. The model is a simplified version of a code used for the ITER magnets [5], [11]. The conductor AC losses are treated as the sum of two components—hysteresis and coupling, each of which can be assessed independently. The magnetic field B is computed at a representative number of points placed over the coil length (one point per turn in the case at hand). Then the code analyzes field evolution and conductor operating conditions (transport current scenario, conductor temperature, which can vary both over the coil length and with time, and the filament strain ε) at each observation point, for the computation of the loss components.

The experimental database, provided by strand/cable manufacturers gives, in addition to the conductor geometrical data (cable layout, strand diameter, Cu : non-Cu ratio, cross sections, etc.), measured values of the noncopper critical current density (at 12 T, 4.2 K, $\varepsilon = -0.25\%$) and of the hysteresis loss energy for a standard (± 3 T) pulse. For the CSIC witness strand, these are 685 A/mm^2 and 92 mJ/cm^3 respectively. The effective filament diameter estimated using these two characteristic values, and used for the hysteresis loss assessment, is about 5–5.2 μm. The hysteresis losses in the CSMC and CS Insert conductors were measured during very slow current ramps ($\sim$1 kA/min). During relatively fast test pulses (i.e., for dB/dt $>$ 0.3 T/s) the total losses in the CSIC are dominated by the coupling component.

A convenient and common way to assess the coupling losses in a coil is to employ the effective time constant ($n\tau$). However, a definition of the time constant for a multistage cable is not so obvious. It ranges from a scaling coefficient, which value can be found from the linear part of the loss vs. frequency (field rate) plot, to a function combining several dominant time constants interacting by shielding with weighted volume fractions [12]. An accurate prediction of $n\tau$ value for a cable is even more complicated. Estimations of $n\tau$ were carried out during a series of loss measurements performed with short samples of ITER sub- and full-size cables and ITER relevant coils before the CSMC/CSIC test campaign. The following tendencies of $n\tau$ behavior were observed.

- A single time constant could hardly give a good accuracy of loss assessment over an extended range of ITER-relevant field rates (from 0 to 1–2 Hz frequency) [12]. In other words, the apparent time constant appeared to be "field rate dependent" [13], [14].
- It was found [12] that the losses in a cable loaded with mechanical pressure (or Lorentz force $I \times B$) were gradually decreasing with the number of loading cycles until they finally settled at a certain level.
- Even the "settled" $n\tau$ remained "transverse load sensitive": the larger was the transverse force applied, the higher were the losses produced by a conductor under a pulsed field [12].

To a certain extent all the above-mentioned effects were seen during the CSMC and CS Insert test [3]. Depending on the test conditions, the estimated $n\tau$ values for the CSIC range from 15 ms [15]—relatively fast pulse with the Insert carrying no current, to over 50 ms [3]—relatively slow discharge and rather high current/field level.

The coupling losses are simulated here with a single $n\tau$. However, two approaches are suggested. The first approach is to find a value of $n\tau$ that would give a good fit for the total loss energy generated over the considered field pulse. As the selected test conditions here are "relatively fast ($dB/dt \sim 1$ T/s) full current pulse" the probable $n\tau$ figure should be around 25–30 ms. The second one is an attempt to introduce a certain "τ-function," which would reflect the major tendencies of the apparent $n\tau$ behavior: field rate and transverse load dependence. This is supposed to give a better picture of loss evolution during the test pulse. For the first try we use the following simple model:

$$n\tau(t) = k_1(\text{force}) \times k_2(\text{load\_history}) \times 2\tau(\chi)$$

where k_1 and k_2 are correction coefficients responsible for the applied transverse load and the conductor load history, and $\tau(\chi)$ is a function of the field rate χ (T/s). The transverse load coefficient can be written as

$$k_1 = 0.5\,\{1 + [I(t) \times B(t)]/[I_{\max} \times B_{\max}]\}$$

where $I_{\max} \times B_{\max} = 13\ \mathrm{T} * 46\ \mathrm{kA} = 600$ kN/m. The "load history" coefficient (k_2) for the given case can be taken as 1. Finally, the $\tau(\chi)$-function can be written as

$$\tau = \tau_{\inf} + \tau_0 \times \exp(-\chi/\alpha)$$

where $\tau_{inf} = 5$ ms corresponds to the time constant at a "very high frequency," $\alpha = 1$ T/s, and τ_0 is a fitting parameter.

C. Coupling Between Thermal-Hydraulic and AC Losses Model

The coupling between the two models must have in principle an iterative structure, as the hysteresis losses depend on the strand temperature, whose evolution is in turn due to the total losses. However, in view of the above-mentioned limited weight of hysteresis vs. coupling, this feedback is not too strong. Therefore, we proceed as follows: a first space and time dependence of the losses (W/m) is computed with the AC losses code using a "reasonable" guessed evolution of the temperature profile along the conductor; then, a full transient (up to the selected final time) is computed with M&M, using the just computed losses as the driver; new AC losses are then computed using the temperature evolution computed by M&M at the previous iteration, and the full transient is re-computed with M&M using the new losses. These two steps are typically enough for convergence, loss power variations between iterations being restricted to the second or third digit for the case at hand.

IV. Results and Discussion

We begin with the analysis of *shot 301-1*, a RRL test performed on July 20, 2000, in a sense the most performing pulsed shot of the CSIC test campaign. The CSIC and the CSMC were connected in series, and the transport current I was increased at a rate of ~4.1 kA/s (equivalent to $dB/dt \sim 1.2$ T/s) up to a maximum current of ~44.3 kA, see Fig. 3(a). As the plateau was reached the CSMC quenched and after ~1 s delay a manual dump of the current was performed, but no quench was revealed in the CSIC. Here we shall restrict our analysis to the first minute of the CSIC transient, covering the whole current pulse, so that the *direct* effects of AC losses can be observed.

In the AC losses model we use $n\tau\ (t)$ in the CSIC, with $n\tau_0 = 100$ ms (equivalent to $n\tau \sim 30$ ms = constant in terms of total energy deposited), while $n\tau = 50$ ms = constant is used in the CSMC [3]. (For the "average" CSMC conductor the field map of layer 1 is used.) The computed time evolution of the losses near the center of the conductors is shown in Fig. 3(a).

The first thermal-hydraulic effects of the AC losses in the CSIC strands are the heating of the conductor components and the resulting pressurization of the SHe. A comparison between computed and measured temperatures and pressures is shown in Fig. 3(b), (c), respectively. The qualitative evolution is correctly reproduced by the code, although the "final" values are somewhat overestimated. The overshoot of p_{ctr} near the end of the ramp-up, as well as the overshoot of T_{ctr}, near the beginning of the dump, are both not captured by the simulation, possibly indicating that the AC loss model might be inadequate during these phases.

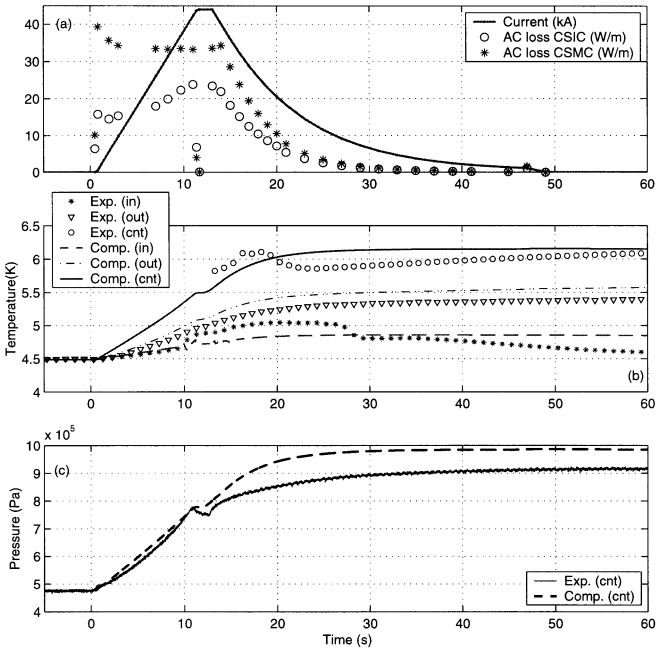

Fig. 3. (a) Measured transport current scenario, and computed losses in the center of the CSIC and of the "average" CSMC conductor. (b) Computed and measured CSIC temperatures. (c) Computed and measured CSIC pressures.

The second thermal-hydraulic effect of AC losses on the CSIC is to induce a repartition of the helium flow among the different parallel channels, based on their different losses and hydraulic characteristics. Let us first of all consider the evolution of the sum of the inlet mass flow rates in all *CSMC* inner module conductors (G_{in}^{IM}), its counterpart in the outer module (G_{in}^{OM}), and the total inlet mass flow rate in the system (G_{in}^{tot}), as shown in Fig. 4(a). It is clearly seen that strong losses in the inner module, where the field is higher, lead to a strong reduction of G_{in}^{IM} and this, with a possibly approximately constant G_{in}^{tot}, leads to a strong increase of G_{in}^{OM} in the first phase of the transient. As to the *CSIC*, the evolution of its inlet mass flow rate G_{in}^{CSIC} is shown in Fig. 4(b). After a small, almost unnoticeable reduction, G_{in}^{CSIC} increases in the initial phase of the ramp-up, somewhat contrary to intuition, and only eventually it starts decreasing as expected, because of the losses *in the CSIC* itself. The initial increase of G_{in}^{CSIC} is due to the strong decrease of G_{in}^{IM} at G_{in}^{tot} constant, as is confirmed by the fact that in this phase the helium temperature T_{in}^{CSIC} is also increasing [see Fig. 3(b)], possibly because of mixing with the hot helium being expelled at the inlet of the innermost CSMC layers. However, in this phase of the transient the *variations* of the CSIC inlet mass flow rate (of the order of 1 g/s) come from differences of much larger quantities (of the order of ~100 g/s), see Fig. 4, and as such they are rather sensitive to external factors.

Toward the end of the ramp-up, a strong change in the slope of G_{in}^{CSIC} is observed (synchronous with the above-mentioned overshoot in p_{ctr}) and backflow at the CSIC inlet is revealed

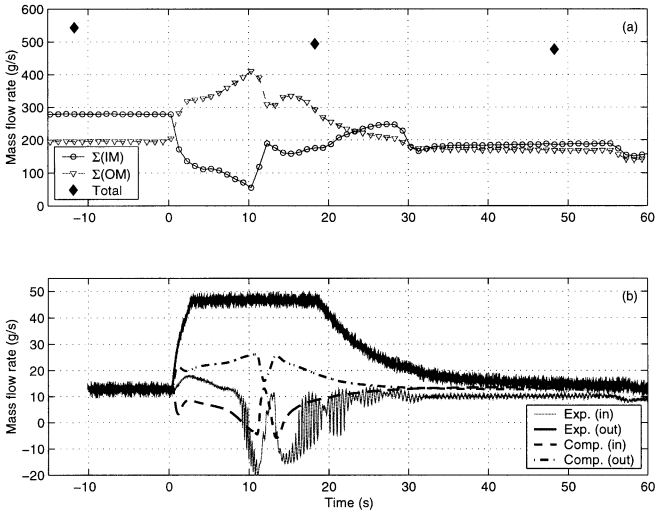

Fig. 4. Evolution of the mass-flow rate. (a) Measured totals at coil inlet (CSV_FRT_CB40XB), at inner module (IM) inlet and at outer module (OM) inlet. (b) Computed and measured at CSIC inlet and outlet.

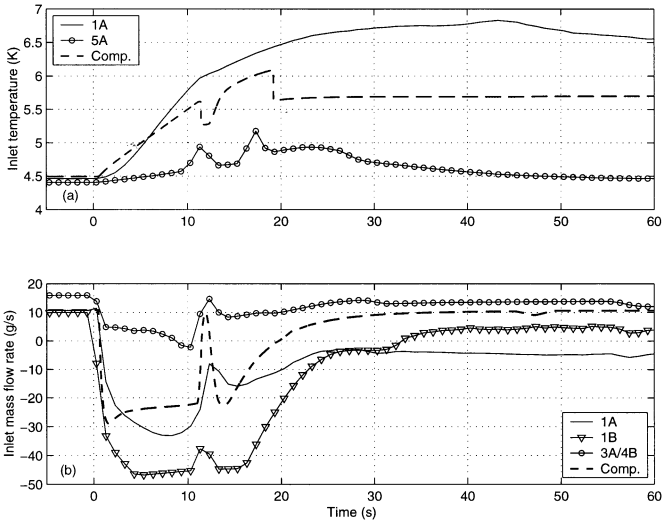

Fig. 5. Evolution of CSMC parameters. (a) Computed and measured inlet temperatures. (b) Computed and measured inlet mass flow rates.

bythe flow meter. This change in slope is not observed in other, similar CSIC shots with lower ramp rate (e.g., shot 250-1 at 0.4 T/s, see below, or shot 255-1 at 0.6 T/s), and can hardly be explained in terms of normal coil operation. It might be related to different phenomena appearing at high ramp rate. As the losses go to zero during the current flat top, G_{in}^{CSIC} recovers, and then decreases again because of the losses in the CSIC associated with the current dump. The outlet mass flow rate G_{out}^{CSIC} is also shown in Fig. 4(b) and quickly increases up to saturation of the signal.

The computed evolution of G_{in}^{CSIC} and of G_{out}^{CSIC} is also shown in Fig. 4(b). Although most of the qualitative features of the transient are recovered, one cannot claim a quantitative agreement. The computed G_{in}^{CSIC} shows an initial reduction (overestimated with respect to the experiment) due to the losses in the CSIC, then increases, as discussed above for the experimental signal, until the losses in the CSIC do not prevail again, leading to a further reduction (underestimated with respect to the experiment). We see a change in slope in the mass flow rate reduction but far smaller than measured. The model qualitatively reproduces the dump phase of the transient. G_{in}^{CSIC} computed using experimental boundary conditions (not shown) is qualitatively similar (also in the disagreement with the experiment) to that obtained from the full circuit model. The computed G_{out}^{CSIC} appears to strongly underestimate the measured values, and we cannot explain the curious asymmetric behavior measured with respect to the inlet.

The measured and computed transients at the inlet of the "average" CSMC inner layer conductor are compared in Fig. 5. Both the computed T [see Fig. 5(a)] and the computed G [see Fig. 5(b)] are in qualitative agreement with the average of the corresponding values, measured at the inlet of the innermost CSMC layers.

To assess what of the previous qualitative features may be related to the very fast ramp rate, we have also analyzed *shot 251-1*, a RRL test completely analogous to shot 301-1, except $dB/dt \sim 0.4$ T/s is much slower. The corresponding current scenario and computed losses are shown in Fig. 6(a),

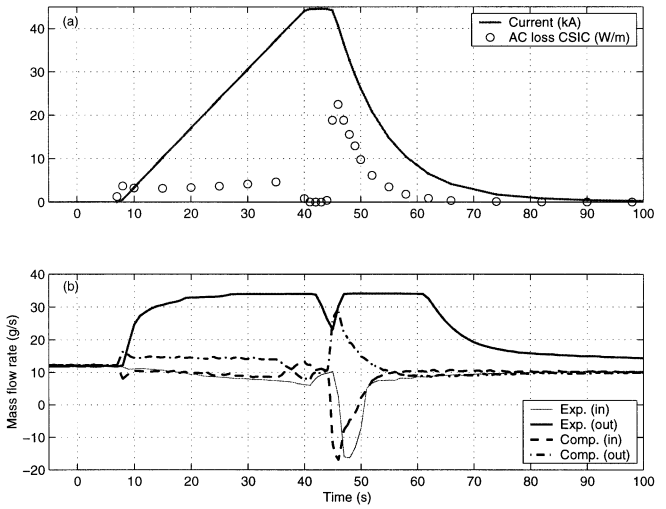

Fig. 6. Shot 250-1. (a) Measured transport current scenario, and computed losses in the center of the CSIC conductor. (b) Computed and measured mass flow rates.

and the comparison between measured and computed (with experimental boundary conditions, but otherwise the same input parameters) mass flow rates is shown in Fig. 6(b). It is seen that the much lower losses during the ramp cause a much smaller reduction of G_{in}^{CSIC}, which is well reproduced by the code, without change in slope. G_{out}^{CSIC} increases again very strongly and somewhat unexplained, see also [10]. The strong inlet backflow due to the losses during the dump is also well reproduced by the code, indicating that most of the unexplained features during the ramp-up of shot 301-1 should indeed be peculiar to the fast dB/dt. The central temperature evolution (not shown) is a little underestimated by the code.

V. Conclusion and Perspective

A detailed model for AC losses has been implemented in the M&M code and the resulting tool has been applied for the first time to an analysis of the most performing CSIC pulsed shot (field ramp-up rate ∼1.2 T/s, followed by a fast manual dump

with time constant of ∼9 s). The main thermal-hydraulic effects of the AC losses are qualitatively reproduced by the code, while quantitative agreement is very difficult to obtain particularly for the mass flow rate. By comparison with a lower dB/dt shot it was shown that some qualitative features and difficulties for the modeling appear indeed related to the high field rate, while G_{in}^{CSIC} was reproduced.

We plan to apply the same tool to the analysis of the thermal-hydraulic effects of AC losses in the CSMC, and to the analysis of the so-called "big" quench of the CSIC.

ACKNOWLEDGMENT

The authors thank Y. Takahashi for several discussions and Fig. 1.

REFERENCES

[1] H. Tsuji *et al.*, "Progress of the ITER central solenoid model coil program," *Nucl. Fusion*, vol. 41, pp. 645–651, 2001.

[2] T. Kato *et al.*, "First test results for the ITER central solenoid model coil," *Fus. Eng. Des.*, vol. 56–57, pp. 49–60, 2001.

[3] N. Martovetsky *et al.*, "Test of the ITER central solenoid model coil and CS insert," *IEEE Trans. Appl. Supercond.*, vol. 12, pp. 600–605, 2002.

[4] L. Savoldi and R. Zanino, "M&M: Multi-conductor Mithrandir code for the simulation of thermal-hydraulic transients in superconducting magnets," *Cryogenics*, vol. 40, pp. 179–189, 2000.

[5] D. Bessette *et al.*, "Conductors of the ITER magnets," *IEEE Trans. Appl. Supercond.*, vol. 11, pp. 1550–1553, 2001.

[6] L. Savoldi and R. Zanino, "Analysis of T_{cs} measurement in conductor 1A of the ITER central solenoid model coil using the M&M code," *Cryogenics*, vol. 40, pp. 593–604, 2000.

[7] ——, "Predictive study of current sharing temperature test in the toroidal field model coil without LCT Coil using the M&M code," *Cryogenics*, vol. 40, pp. 539–548, 2000.

[8] R. Zanino *et al.*, "Inductively driven transients in the CS insert coil (I): Heater calibration and conductor stability tests and analysis," *Adv. Cryo. Eng.*, vol. 47, pp. 415–422, 2002.

[9] L. Savoldi, E. Salpietro, and R. Zanino, "Inductively driven transients in the CS insert coil (II): Quench tests and analysis," *Adv. Cryo. Eng.*, vol. 47, pp. 423–430, 2002.

[10] H. Takigami *et al.*, "Predicted thermohydraulic performance of the ITER central solenoid model coil conductors," *IEEE Trans. Appl. Supercond.*, vol. 10, pp. 1070–1073, 2000.

[11] N. Mitchell *et al.*, "Appendix C: Superconducting magnet design criteria," ITER N11 DDD 32 97-12-08 W 0.2, DD1.1-1.3.

[12] A. Nijhuis *et al.*, "Electromagnetic and mechanical characterization of ITER CSMC conductor affected by transverse cyclic loading, Part 1: Interstrand coupling losses," *IEEE Trans. Appl. Supercond.*, vol. 9, pp. 1069–1072, 1999.

[13] P. L. Bruzzone *et al.*, "Test results for the high field conductor of the ITER central solenoid model coil," *Adv. Cryo. Eng.*, vol. 45, pp. 729–735, 2000.

[14] D. Ciazynski *et al.*, "Test results and analysis of two european full-size conductor samples for ITER," *IEEE Trans. Appl. Supercond.*, vol. 10, pp. 1058–1061, 2000.

[15] Y. Takahashi *et al.*, "AC loss measurement of 46kA-13T Nb3Sn conductor for ITER," *IEEE Trans. Appl. Supercond.*, vol. 11, pp. 1546–1549, 2001.